Journal of Solid State Chemistry **145,** 471–478 (1999)
Article ID jssc.1998.8159, available online at http://www.idealibrary.com on IDEAL®

Pressure and Temperature Evolution of the Structure of the Superconducting Na_2CsC_{60} Fulleride

Serena Margadonna,* Craig M. Brown,*,† Alexandros Lappas,* Kosmas Prassides,*,[1] Katsumi Tanigaki,‡ Kenneth D. Knudsen,§,‖ Tristan Le Bihan,‖ and Mohamed Mézouar‖

*School of Chemistry, Physics and Environmental Science, University of Sussex, Brighton BN1 9QJ, United Kingdom; †Institut Laue Langevin, B.P. 156, F-38042 Grenoble Cedex 9, France; ‡Department of Material Science, Faculty of Science, Osaka City University, 3-3-138 Sugimoto, Sumiyoshi-ku, Osaka 558-8585, Japan; §Institute of Crystallography, University of Lausanne, CH-1015 Lausanne, Switzerland; and ‖European Synchrotron Radiation Facility, B.P. 220, F-38043 Grenoble, France.
E-mail: K.Prassides@susx.ac.uk

Received October 26, 1998; accepted December 10, 1998

DEDICATED TO PETER DAY ON HIS 60TH BIRTHDAY

The structural properties of the Na_2CsC_{60} fulleride have been studied by synchrotron X-ray powder diffraction at both ambient and elevated pressures. Complementary neutron diffraction measurements at high pressure were also performed. We find no evidence for a monomer → polymer phase transition on cooling at ambient pressure, despite the adopted slow cooling procedures, with the structure remaining strictly cubic, even after prolonged standing at 200 K. The pressure dependence of the structure of solid Na_2CsC_{60} at ambient temperature was followed up to 0.56 GPa by neutron diffraction and up to 8.63 GPa by synchrotron X-ray diffraction. At ambient pressure, the structure is primitive cubic with $a=14.1329(3)$ Å (space group $Pa\bar{3}$). When a pressure of 0.76 GPa is reached, an incomplete phase transition to a low-symmetry structure, accompanied by a large volume decrease (2.7(1)%), is encountered. This phase was characterized as monoclinic with $a=13.745(5)$ Å, $b=14.224(6)$ Å, $c=9.408(3)$ Å, and $\beta=133.71(1)^\circ$ (space group $P2_1/a$), isostructural with the low-temperature polymer phase of Na_2RbC_{60}. The cubic and polymeric phases of Na_2CsC_{60} coexist up to 0.90 GPa. The pressure evolution of the monoclinic lattice constants *a*, *b*, and *c* to 8.63 GPa reveals the presence of substantial anisotropy in the compressibility along the three axes. The structure is least compressible along the *c* axis, which defines the polymeric C–C bridged fulleride chains and is most compressible along the interchain *b* direction. © 1999 Academic Press

INTRODUCTION

The series of ternary alkali fullerides with stoichiometry, $A_2A'C_{60}$ (A, A' = alkali metal) can be classified into different structural families, distinguished through the orientational state adopted by the C_{60}^{3-} ions in the crystal structure (1–4). K_3C_{60} and Rb_3C_{60} have a merohedrally disordered face-centered cubic (fcc) structure (space group $Fm\bar{3}m$) in which the C_{60}^{3-} ions are randomly distributed between two orientations related by 90° rotation about the cubic axes and do not undergo any phase transition with change in temperature (5). Geometrical considerations reveal that, while the size of the octahedral holes ($r_0 \sim 2.06$ Å) is large enough to accommodate any alkali ion, the tetrahedral hole ($r_t \sim 1.12$ Å) is smaller than the ionic radii of K^+, Rb^+, and Cs^+. As a result, rotational motion of the fulleride ions is restricted and the A^+–C_{60}^{3-} orientational potential is dominated by repulsive interactions. On the other hand, the Na^+ ionic radius (~0.95 Å) is smaller than the size of the tetrahedral interstices, so the C_{60}^{3-} ions are no longer confined to the two standard orientations, found in K_3C_{60}; instead, there is enough space for them to rotate in such a way as to optimize both the attractive Na^+–C_{60}^{3-} and the C_{60}^{3-}–C_{60}^{3-} interactions. As a consequence, the Na_2AC_{60} ($A = K^+$, Rb^+, Cs^+) fullerides adopt an orientationally ordered primitive cubic (space group $Pa\bar{3}$) structure just below room temperature, in which the majority of the fulleride ions are rotated counter-clockwise by ~98° about the appropriate [1 1 1] cube diagonal, with the remaining ions adopting minor orientations (6, 7). In all these cases, the structures remain three-dimensional with typical nonbonding interfullerene distances in excess of 3 Å.

This simple picture of interfullerene bonding in intercalated fullerides changed drastically when a conducting phase with stoichiometry AC_{60} (A = K, Rb, Cs) that exhibited quasi-one-dimensional character and unusually close interfullerene contacts was identified (8). Structural characterization of these phases established the formation of C_{60}^- polymer chains with fulleride linkages achieved by a [2 + 2] Diels–Alder cycloaddition mechanism which results in the

[1] To whom correspondence should be addressed.

0022-4596/99 $30.00

formation of four-membered carbon rings, fusing together adjacent molecules. Such types of bridged fullerene structures also occur in photo- (9) and high-pressure (10, 11) polymerized C_{60} and were originally considered to be quite exotic. However, the family of bridged dimeric and polymeric fullerene intercalated compounds has currently grown considerably (12) to include covalently bridged C_{60}^{3-} ions in Na_2AC_{60} (A = K, Rb, Cs) salts (13) and C_{60}^{4-} ions in the Na_4C_{60} salt (14).

The formation of polymerized structures by C_{60}^{3-} ions in fulleride salts both at ambient (13) and elevated (15) pressure is of particular interest, as it is for the same compositions that superconductivity is also encountered. Fulleride salts with stoichiometry, $A_2A'C_{60}$ (A, A' = alkali metal) exhibit superconductivity with T_c as high as 33 K at ambient pressure (16). Moreover, the transition temperature, T_c scales monotonically with the cubic unit cell size, a_0 (17); this observation can be rationalized in terms of the increasing density of states at the Fermi level, $N(\varepsilon_F)$ with increasing interfullerene separation, resulting from the decrease in the overlap between the molecules that leads to band narrowing. Deviations from this behavior have been encountered at small interfullerene separations for the $Pa\bar{3}$ family of sodium fullerides, $Na_2Rb_{1-x}Cs_xC_{60}$ ($0 \leq x \leq 1$) in which the rate of decrease of T_c with interfullerene spacing is found to be considerably steeper (18). While earlier work (7, 18) favored an explanation of this behavior in terms of the modified crystal structures and the different orientational state of C_{60}^{3-} ions in the $Pa\bar{3}$ phases, subsequent EPR (19–21) and NMR (22) measurements found little difference in the a_0 dependence of $N(\varepsilon_F)$ between Na_2CsC_{60} ($Pa\bar{3}$) and K_3C_{60} or Rb_3C_{60} ($Fm\bar{3}m$) to justify such a conjecture. This was further reinforced by the results of high-pressure susceptibility measurements which revealed that both Na_2CsC_{60} (20, 23) and $Na_2Rb_{0.5}Cs_{0.5}C_{60}$ (24) show an evolution of T_c with interfullerene spacing comparable to that of K_3C_{60}.

Careful measurements on the Na_2KC_{60} and $Na_2Rb_{1-x}Cs_xC_{60}$ ($0 \leq x \leq 1$) series have now established that superconductivity is associated with the metastable $Pa\bar{3}$ phases which survive to low temperatures (13, 25). The true ground state of the system at low temperature, obtained after extremely slow cooling procedures, is not superconducting and adopts a monoclinic structure while comprises of quasi-one-dimensional chains of C_{60}^{3-} ions, bridged by single C–C bonds and with short interball center-to-center distances ($\approx$9.3–9.4 Å) (13, 25–28). While the rapidly suppressed values of T_c in $Na_2Rb_{1-x}Cs_xC_{60}$ ($0 \leq x \leq 1$) may well arise from reasons purely associated with the primitive cubic phases (distortion, electron transfer) (1,24), there exists the possibility that they may be also related to the co-existence at the microscopic level of superconducting cubic and non-superconducting polymer domains whose size varies with x. Actually the formation of the polymer structure appears to depend very sensitively on the interfullerene separation and attempts to form a polymer phase at ambient pressure for the member of the series with the largest cubic lattice constant, Na_2CsC_{60} have been unsuccessful (13, 25).

In order to explore the conditions under which polymerisation is encountered in Na-containing primitive cubic fullerides, we performed detailed powder diffraction measurements on Na_2CsC_{60} both as a function of temperature at ambient pressure (by the synchrotron X-ray technique) and as a function of pressure at ambient temperature (by the synchrotron X-ray and neutron techniques). No evidence for polymerization has been found at ambient pressure with Na_2CsC_{60} remaining strictly cubic. Upon the application of pressure, the primitive cubic phase also survives to 0.90 GPa. However, at a pressure of 0.76 GPa, an additional low-symmetry phase appears; it grows at the expense of the cubic phase up to 0.90 GPa, and then survives to the highest pressure of the present experiments (8.63 GPa). The high-pressure phase of Na_2CsC_{60} has been structurally characterised to be monoclinic and isostructural with the ambient pressure low-temperature polymer phase of Na_2RbC_{60}.

EXPERIMENTAL

(a) Synthesis

The Na_2CsC_{60} sample used in the present work was prepared by reaction of annealed C_{60}, with stoichiometric quantities of Na and Cs metals. These were contained in a tantalum cell which was placed inside a sealed glass tube filled with He to 600 Torr. The reactants were heated at 200°C for 12 h and at 430°C for 3 weeks with intermittent shakings. Phase purity was confirmed by X-ray diffraction with a Siemens D5000 diffractometer.

(b) Temperature Dependent Synchrotron X-Ray Diffraction Experiments

Synchrotron X-ray diffraction measurements on the sample sealed in a thin-wall glass capillary 0.5 mm in diameter were performed on the Swiss-Norwegian beamline (BM1A) at the European Synchrotron Radiation Facility, Grenoble, with a 300 mm diameter Mar Research circular image plate (150 μm pixel size). A monochromatic X-ray beam of wavelength, $\lambda = 0.8729$ Å and dimensions 0.50×0.50 mm^2 was focused onto the sample by sagittal bending of the second crystal of the double-crystal Si (1 1 1) monochromator. The sample was cooled from 320 to 200 K at a rate of 60 K/h, where it was kept for 6 hours. Cooling was by means of an Oxford Cryosystems Cryostream cold nitrogen blower. Images of the Debye–Scherrer rings were measured every 6 min with a sample-to-detector distance of 300 mm and with an exposure time of 2 min. During the data collection the sample was rotated about its axis by 30°.

One-dimensional diffraction patterns were obtained by integrating around the rings using local software (program FIT2D). Data analysis was performed with the FULLPROF suite of Rietveld analysis programs (29).

(c) Pressure Dependent Synchrotron X-Ray and Neutron Diffraction Experiments

The high-pressure X-ray diffraction experiments at ambient temperature were performed on beamline ID30 at the European Synchrotron Radiation Facility, Grenoble. The same Na_2CsC_{60} powder sample was loaded in a diamond anvil cell (DAC), which was used for the high-pressure generation and was equipped with an aluminum gasket. The diameters of the two faces of the diamond culet were 350 and 500 μm, and the sample was introduced in a hole made in the gasket 80 μm deep and 200 μm diameter. Silicone oil loaded in the DAC was used as a pressure medium. Pressure was increased at room temperature and was measured with the ruby fluorescence method. The diffraction patterns were collected using an image plate detector ($\lambda = 0.6364$ Å) up to a maximum pressure of 8.63 GPa. Masking of the strong Bragg reflections of the ruby chip and integration of the two-dimensional diffraction images were performed with the local ESRF FIT2D software. Data analysis was performed with the PROFIL suite of Rietveld analysis programs (30).

Neutron diffraction experiments were performed on the POLARIS high-intensity powder diffractometer at the ISIS spallation neutron source, Rutherford Appleton Laboratory, UK. For the present high-pressure diffraction measurements, the low-angle detector bank at fixed scattering angle, $2\theta = 35°$, was used to collect data in the d-spacing range of 0.8–8.0 Å. A TiZr null-matrix alloy cell (diameter = 5 mm) with Ar gas as pressure transmitting medium ($P_{max} = 0.7$ GPa) was employed. Because of the small sample mass (≈ 200 mg) and the weak scattered intensity, no B_4C collimator for the incident and scattered beams—commonly employed to eliminate possible contamination of the diffraction pattern by Bragg peaks from the TiZr cell components—was used. Still it proved necessary to use relatively long counting times in order to obtain acceptable statistics. For instance, the counting time for the dataset at ambient pressure was 18 h (total current ≈ 2.9 mA). The measured diffraction profiles at $P = 0.11$, 0.21, 0.30, 0.45, and 0.56 GPa were each collected over a period of 6 h. A diffraction dataset of the empty TiZr cell was also collected over the same period. The data within the 35° detector bank were summed and corrected for attenuation and multiple scattering. Following subtraction of the empty cell contribution, they were then normalized to a standard vanadium run. The incident neutron flux contribution was also removed before further treatment with the ISIS powder diffraction software (31).

RESULTS

(a) Structural Results at Ambient Pressure

Synchrotron X-ray powder diffraction profiles of Na_2CsC_{60} were collected on slow cooling from 320 to 200 K at ambient pressure (Fig. 1). The cooling protocol was similar to that used before in our structural work on Na_2RbC_{60} which showed a slow, incomplete phase transition from the primitive cubic to the monoclinic polymer structure in the vicinity of 250 K (32, 33). In the present case, the Na_2CsC_{60} sample adopts a fcc structure at temperatures above 290 K. In the vicinity of 290 K, a sudden shift in the position of the cubic peaks to larger 2θ values and a discontinuity in the rate of lattice contraction are encountered, signaling the well-known fcc-to-primitive cubic orientational ordering transition (7). No evidence for additional diffraction peaks violating cubic symmetry is apparent down to 200 K, even after standing at this temperature for 6 h.

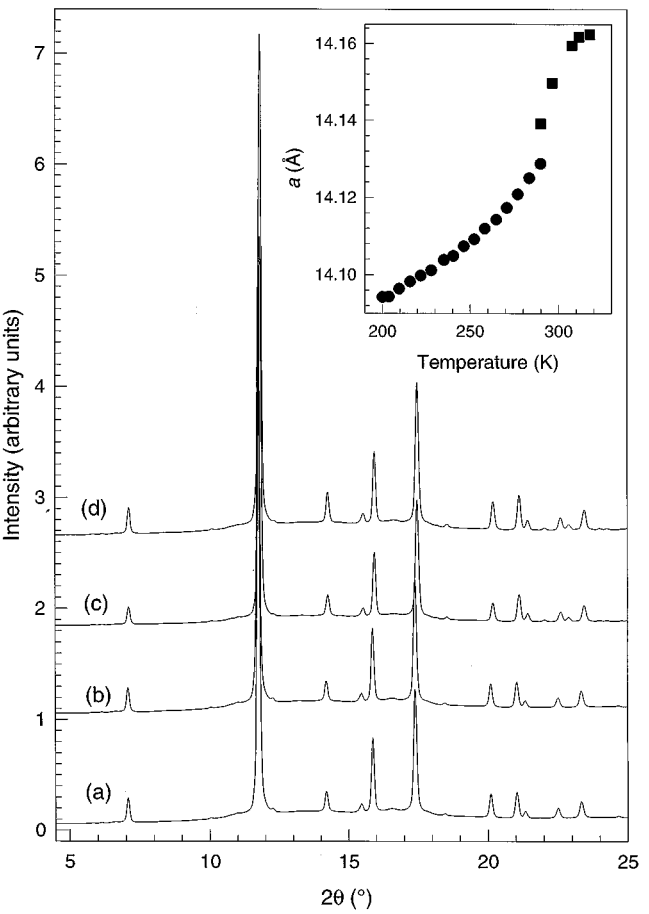

FIG. 1. Synchrotron X-ray ($\lambda = 0.8729$ Å) powder diffraction profiles of Na_2CsC_{60} at various temperatures: (a) 317.4 K, (b) 289.9 K, (c) 203.4 K. The top pattern (d) was obtained after staying at 200 K for 6 h. Inset: Temperture dependence of the cubic lattice constant of Na_2CsC_{60} obtained on cooling.

For the diffraction data collected down to 290 K, Rietveld refinements were performed with the fcc structural model (space group $Fm\bar{3}m$) in which the C_{60}^{3-} ions are modeled as quasi-spherical orientationally disordered units of radius, $R = 3.55$ Å and the Na^+ and Cs^+ ions are placed in the 8*c* ($\frac{1}{4}$, $\frac{1}{4}$, $\frac{1}{4}$) and 4*b* ($\frac{1}{2}$, $\frac{1}{2}$, $\frac{1}{2}$) sites of the unit cell, respectively (at 317.7 K: lattice constant, $a = 14.1642(7)$ Å; agreement factors, $R_{wp} = 12.2\%$, $R_{exp} = 3.3\%$). At temperatures below 290 K, the primitive cubic structural model (space group $Pa\bar{3}$) was employed in which the C_{60}^{3-} units are rotated away from their standard orientations counter-clockwise about the [1 1 1] cube diagonal directions by either $\phi \sim 98^\circ$ or 38°. The Na^+ and Cs^+ ions are placed in the 8*c* (*x*, *x*, *x*) and 4*b* ($\frac{1}{2}$, $\frac{1}{2}$, $\frac{1}{2}$) sites of the unit cell, respectively. Using this structural model, the Rietveld refinements, proceeded smoothly down to 200 K (lattice constant, $a = 14.0942(5)$ Å; fractional coordinate, $x = 0.246$; agreement factors, $R_{wp} = 11.8\%$, $R_{exp} = 3.7\%$). The temperature evolution of the cubic lattice constants is shown in the inset of Fig. 1. The thermal expansivity, α of Na_2CsC_{60} is calculated to be $2.20(6) \times 10^{-5}\ K^{-1}$ between 200 and 265 K. The data at 290 K were refined successfully with a two-phase model of co-existing fcc (72(2)%) and primitive cubic (28(2)%) structures with lattice constants, $a = 14.1391(10)$ and 14.1142(6) Å, respectively (agreement factors, $R_{wp} = 12.0\%$, $R_{exp} = 3.4\%$), implying a lattice contraction at the transition temperature of 0.18(1)%.

(b) Structural Results at High Pressure

Powder neutron diffraction results. Neutron powder diffraction profiles of Na_2CsC_{60} were collected at pressures between ambient and 0.56 GPa. No phase change to a low-symmetry structure was apparent with applied pressure within the resolution of the present data (Fig. 2). Extraction of reliable lattice constants was performed using the Pawley method in the *d* spacing range 2.5–6.0 Å. In this procedure, implemented in the local software CAILS, the only parameters refined are cell constants, integrated intensities (in the form of unnormalised structure factors, $|F^2|$) and peak width parameters. The pressure dependence of the lattice constants, extracted from the CAILS refinement of the neutron powder diffraction data, is included in Fig. 5.

Synchrotron X-ray diffraction results. Synchrotron X-ray powder diffraction profiles of Na_2CsC_{60} were collected at pressures between ambient and 8.63 GPa. Inspection of the diffraction data of Na_2CsC_{60} indicated that the pattern could be indexed with a cubic cell at both ambient pressure and at a pressure of 0.61 GPa. The same primitive cubic model (space group $Pa\bar{3}$) of the Na_2CsC_{60} structure that we used at ambient pressure was employed in the refinement of both datasets. Using this model, the Rietveld refinements proceeded smoothly (Fig. 3), leading to values for the cubic

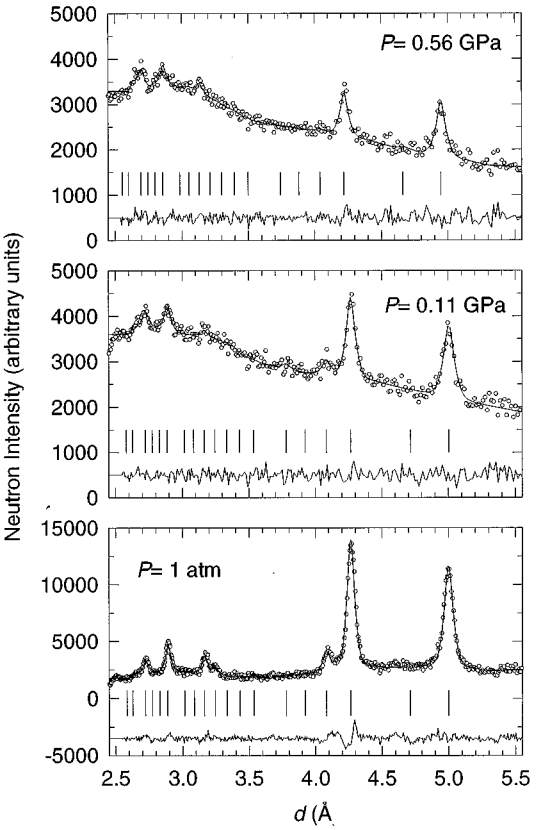

FIG. 2. Observed (points), calculated (solid line), and difference (lower panel) powder neutron diffraction profiles of Na_2CsC_{60} at ambient and elevated ($P = 0.11$ and 0.56 GPa) pressures ($T = 300$ K). The reflection markers are also shown.

lattice constant, $a = 14.133(3)$ Å at ambient pressure ($R_{wp} = 2.6\%$, $R_{exp} = 6.7\%$) and $a = 13.987(5)$ Å at 0.61 GPa ($R_{wp} = 8.2\%$, $R_{exp} = 6.6\%$). The fractional coordinates of the Na^+ ion refine to $x = 0.267(2)$ at ambient pressure and to 0.276(2) at 0.61 GPa, close to the high-symmetry ($\frac{1}{4}$, $\frac{1}{4}$, $\frac{1}{4}$) site encountered in the high-temperature fcc structure of Na_2CsC_{60}. The fractions of the C_{60}^{3-} units in the two orientational states refine to equal values within standard error (52(6)% for $\phi \sim 38^\circ$) at ambient pressure, demonstrating the presence of a high degree of disorder. As the pressure increases to 0.61 GPa, the fraction of the ions in the $\phi \sim 38^\circ$ orientational state decreases to 62(8)%, consistent with its slightly smaller molecular volume that makes it more energetically preferable than the $\phi \sim 98^\circ$ orientational state at higher pressures (34).

When a pressure of 0.76 GPa was reached, the diffraction pattern showed new peaks that could not be accounted for by the primitive cubic structural model. Moreover, these appear to grow with increasing pressure at the expense of the peaks assigned to the low pressure cubic structural model, until they completely dominate the profile at a pressure of 1.12 GPa. A detailed inspection of the profiles suggested that the new Bragg reflections could be indexed with

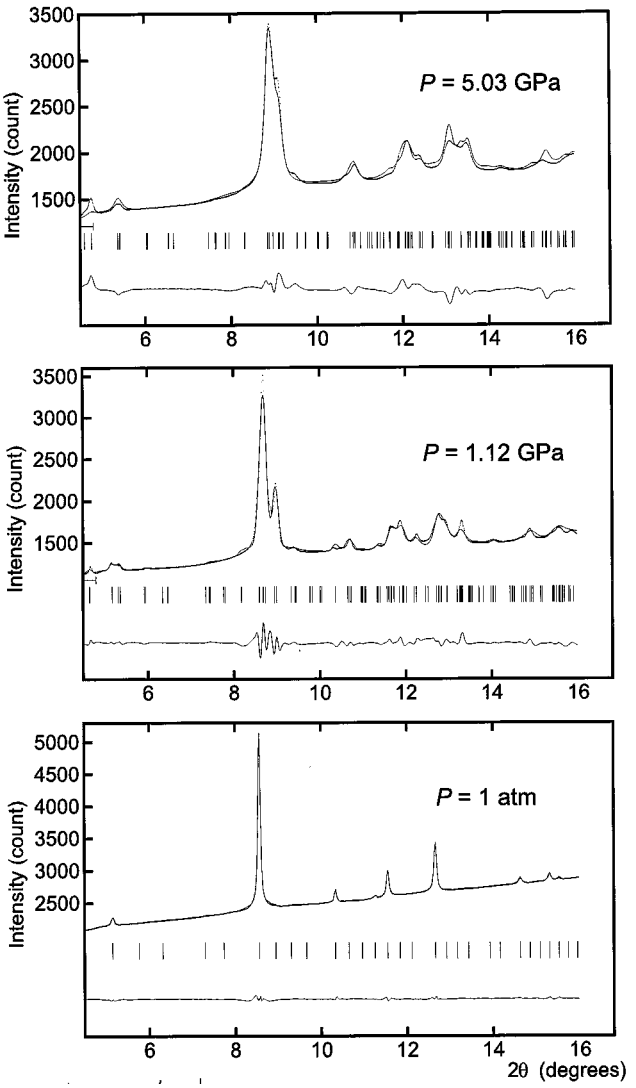

FIG. 3. Observed (points), calculated (solid line), and difference (lower panel) synchrotron X-ray powder diffraction profiles of Na_2CsC_{60} at pressures, $P = 1$ atm and 1.12 and 5.03 GPa ($T = 300$ K). The reflection markers are also shown.

the monoclinic space group $P2_1/a$, used before to describe the polymeric phase of Na_2RbC_{60} formed at low temperatures at ambient pressure. Accordingly, the X-ray powder diffraction profiles at 0.76 and 0.90 GPa were refined by the Rietveld method using a two-phase model of co-existing monoclinic and cubic phases, while for those at pressures between 1.12 and 8.63 GPa, a single phase monoclinic structural model was employed. The latter model was based on the one-dimensional polymeric structure of Na_2RbC_{60} described in previous works (26, 28), in which the fullerene molecules form chains, connected via single carbon–carbon covalent bonds (Fig. 4). Thirty symmetry-inequivalent carbon atoms are needed to generate in space group $P2_1/a$ the two C_{60}^{3-} ions, whose centers reside at the (0, 0, 0) and $(\frac{1}{2}, \frac{1}{2}, 0)$ positions in the unit cell. The orientation of the C_{60}^{3-} ion at (0, 0, 0) is described by an anticlockwise rotation about the [0 0 1] direction of $\psi = 82^\circ$, where the initial orientation of $\psi = 0^\circ$ is that of the standard orientation, located at the origin of an orthorhombic cell defined by the relationships: $a_0 = c_m$, $c_0 = b_m$, and $(a_0/b_0) = \tan(\beta_m - \pi/2)$. In this case, a single C atom is located along the monoclinic c axis which defines the polymer chain axis. The coordinates of the C_{60}^{3-} units were kept constant during refinement at all pressures, with the bridging interfullerene C–C bonds fixed at 1.55 Å. The alkali metals, Cs and Na were located at the $(\frac{1}{2}, 0, 0)$ and $(x \sim 0, y \sim \frac{1}{4}, z \sim \frac{1}{2})$ sites, derived from the high-symmetry octahedral and tetrahedral positions of the parent cubic structure, respectively. The two-phase refinements of the profiles proceeded smoothly (Fig. 3) and the fraction of monoclinic phase increased from 36.7(8)% at 0.76 GPa to 58(1)% at 0.90 GPa. The value of the cubic lattice constant was $a = 13.980(1)$ Å, while those of the monoclinic lattice constants were $a = 13.745(5)$ Å, $b = 14.224(6)$ Å, $c = 9.408(3)$ Å, and $\beta = 133.71(1)^\circ$ at 0.76 GPa ($R_{wp} = 7.6\%$, $R_{exp} = 7.7\%$), showing a decrease in volume of 2.7(1)% on going from the cubic to the monoclinic cell. For pressures in excess of 1.12 GPa, we performed single phase refinements (Fig. 3) with the monoclinic structural model. The lattice constants at 1.12 GPa were $a = 13.718(6)$ Å, $b = 14.078(6)$ Å, $c = 9.396(4)$ Å, and $\beta = 133.69(2)^\circ$ ($R_{wp} = 11.9\%$, $R_{exp} = 9.6\%$). Between 1.12 and 8.63 GPa, the refinements proceeded smoothly, even though with increasing pressure, the peaks became broader and we were able to refine only the lattice parameters. The pressure evolution of the lattice constants of Na_2CsC_{60}, extracted from the Rietveld refinements of the synchrotron X-ray powder diffraction data, is shown in Fig. 5.

DISCUSSION

The temperature dependent synchrotron X-ray data have clearly shown the absence of a phase transition at ambient pressure to a low-symmetry phase in Na_2CsC_{60}, despite the slow cooling procedures adopted. Similar cooling protocols had allowed the primitive cubic (monomer) → monoclinic (polymer) transition to occur on cooling in the vicinity of 250 K for the closely related isostructural fullerides, Na_2KC_{60} and $Na_2Rb_{1-x}Cs_xC_{60}$ ($0 \leq x < 1$). The origin of the differing behavior may be associated with the somewhat increased lattice constant and interfullerene separation in Na_2CsC_{60} (at 246 K, $a = 14.1073(5)$ Å) when compared with the other Na^+-containing fullerides (at 248 K, $a = 14.0808(8)$ Å for Na_2RbC_{60}), implying the presence of a critical contact distance between C_{60}^{3-} ions for C–C bonding to occur. However, the decrease in interfullerene separation between Na_2CsC_{60} and Na_2RbC_{60} is extremely small (only $\approx 0.2\%$) thus, the nonoccurrence of polymerisation in Na_2CsC_{60} on further cooling should

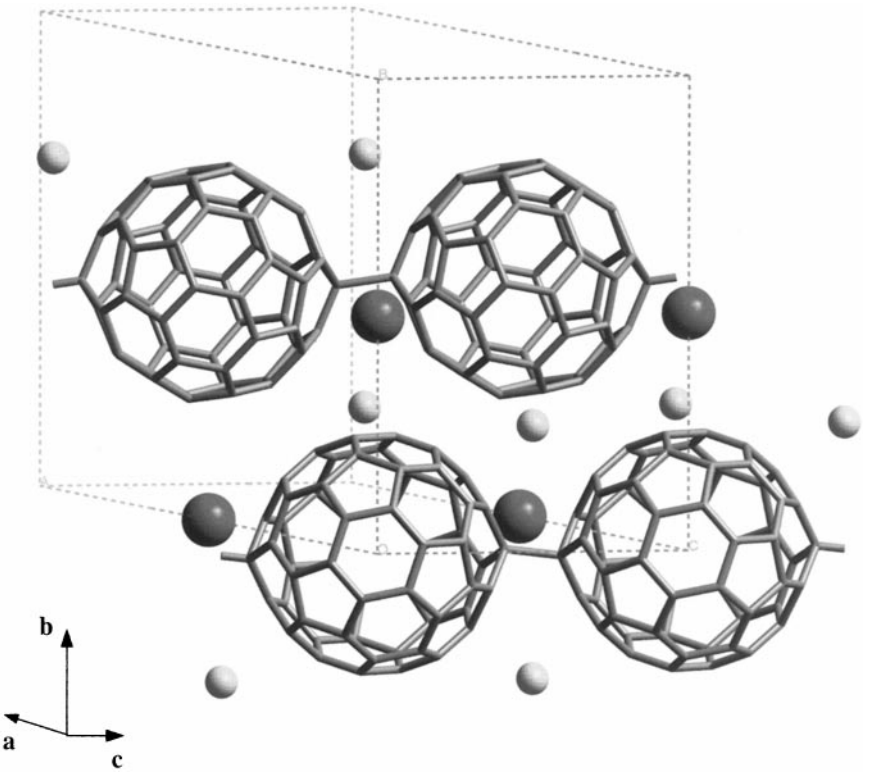

FIG. 4. The crystal structure of polymerized Na_2CsC_{60}. Na^+ and Cs^+ ions are depicted as small and large spheres, respectively.

be also related to kinetic factors. The primitive cubic precursor of the polymer phase is characterized by fullerene orientations in which 6:6 carbon bonds nest over pentagonal faces of neighboring molecules (7). Carbon bonds can then form only during orientational jumps, as the fullerenes perform librational motion (35). As the librational amplitude decreases with decreasing temperature, bond formation becomes rapidly less likely despite the associated lattice contraction which may bring the interfullerene contact distance below the critical value. Such arguments are not applicable when the interfullerene separation is reduced through the application of pressure at room temperature and polymerization can then take place efficiently.

The steric environment of the alkali ions, Na^+ and Cs^+ may also exert an influence on the stability of the tightly packed polymer phase of Na_2CsC_{60}. Each Na^+ ion coordinates to three 6:5 (fusing hexagons and pentagons) C–C bonds and one 6:6 (fusing two hexagons) C–C bond (28). At 1.12 GPa, the shortest Na^+–C_{60}^{3-} approach is ~ 2.53 Å, somewhat smaller than the sum of the van der Waals radius of C (1.65 Å) and the Na^+ ionic radius (0.95 Å) but comparable to that found ($\sim$2.50 Å) at ambient pressure in polymeric Na_2RbC_{60} (28). The average Na^+–C_{60}^{3-} distance is ~ 2.73 Å, presenting no steric crowding. On the other hand, each Cs^+ ion coordinates to four 6:5 and two 6:6 C–C bonds with two shortest Cs^+–C_{60}^{3-} contacts at ~ 3.30 Å and an average distance of $\sim$3.41 Å, identical to those encountered for Rb^+–C_{60}^{3-} in polymeric Na_2RbC_{60}. The steric crowding is however much increased in Na_2CsC_{60}, following replacement of Rb^+ (1.66 Å) by Cs^+, as the sum of the ionic radius of Cs^+ (1.81 Å) and the van der Waals radius of C (1.65 Å) is somewhat larger than the size of the pseudo-octahedral hole occupied.

Figure 6 shows the pressure evolution of the volume of both the cubic and monoclinic structural variants of Na_2CsC_{60}. The volume of the primitive cubic monomer phase varies linearly in the pressure range 0–1 GPa, resulting in a value for the linear volume compressibility of Na_2CsC_{60}, $\kappa \equiv d\ln V/dP = 0.064(4)$ GPa^{-1}. This is larger than those measured for the fcc fulleride phases, K_3C_{60} (0.036(3) GPa^{-1} (36)) and Rb_3C_{60} (0.046(3) GPa^{-1} (36), 0.058(1) GPa^{-1} (37)), a result presumably reflecting the presence of the small Na^+ ions in the tetrahedral interstices and the modified orientational state of the C_{60}^{3-} ions in the primitive cubic solids. Figure 6 also includes a least-squares fit of the ambient-temperature equation-of-state (EOS) of the monoclinic polymer phase of Na_2CsC_{60} to the semi-empirical second-order Murnaghan EOS (38):

$$P = (K_0/K_0')\,[(V_0/V)^{K_0'} - 1], \qquad [1]$$

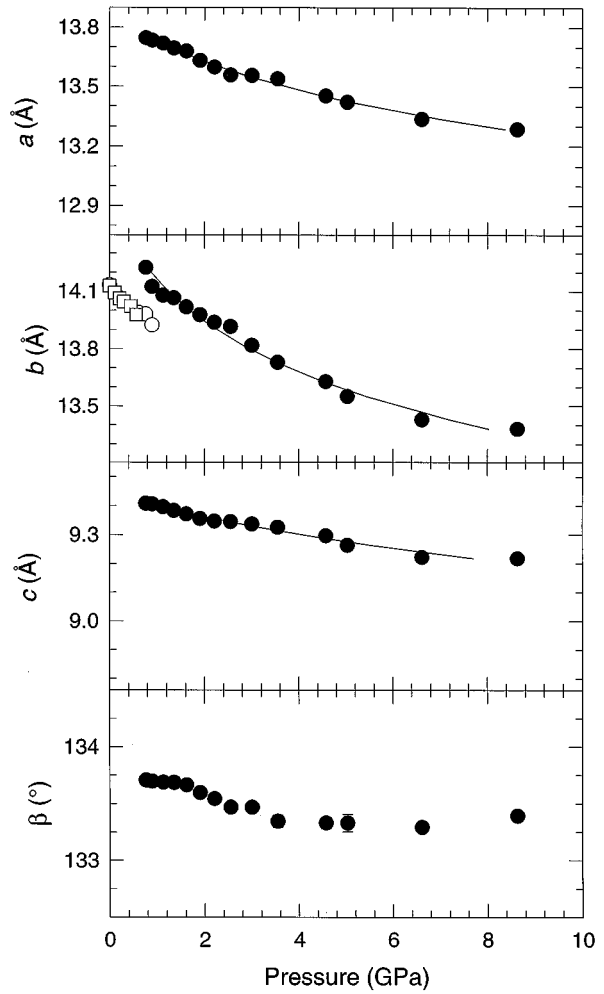

FIG. 5. Pressure dependence of the lattice parameters of the cubic (a) and monoclinic (a, b, c, and β) phases of Na_2CsC_{60} at ambient temperature. Full circles (●) are data for the monoclinic phase obtained by synchrotron X-ray powder diffraction; open circles (○) and squares (□) are data for the primitive cubic phase obtained by synchrotron X-ray and neutron powder diffraction, respectively. The line through the monoclinic phase data represent least-squares fits to the Murnaghan equation-of-state, while that through the cubic phase data is a least-squares linear fit.

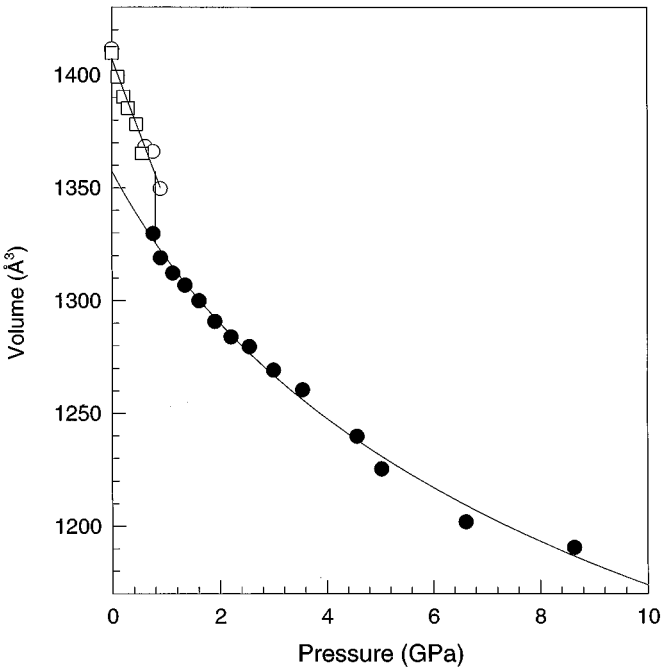

FIG. 6. Pressure dependence of the volume of the cubic ($V/2$) and monoclinic (V) phases of Na_2CsC_{60} at ambient temperature. Full circles (●) are data for the monoclinic phase obtained by synchrotron X-ray powder diffraction; open circles (○) and squares (□) are data for the primitive cubic phase obtained by synchrotron X-ray and neutron powder diffraction, respectively. The line through the monoclinic phase data represents a least-squares fit to the Murnaghan equation-of-state, while that through the cubic phase data is a least-squares linear fit.

where K_0 is the atmospheric pressure isothermal bulk modulus, K_0' is its pressure derivative ($=dK_0/dP$), and V_0 is the unit cell volume at zero pressure. The fit results in values of $K_0 = 28(1)$GPa and $K_0' = 11(1)$. The extracted value of the volume compressibility, $\kappa = 0.037(1)\,\mathrm{GPa}^{-1}$ is smaller than that of the low pressure cubic phase, consistent with the large volume decrease and the tighter average crystal packing of the fulleride ions that accompanies the monomer → polymer phase transition.

The substantial anisotropy in the bonding of the C_{60}^{3-} ions in the monoclinic phase of Na_2CsC_{60} is clearly evident in Fig. 5, which displays the variation of the monoclinic lattice constants a, b, and c with pressure. We described the pressure dependence of each lattice constant with a variant of Eq. [1], in which K_0 and its pressure derivative, K_0' were substituted by the individual K_x and K_x' (x = a, b, c) values. The results of these fits are also included in Fig. 5 and give $K_a = 79.9(5)$ GPa, $K_a' = 37(3)$; $K_b = 25(3)$ GPa, $K_b' = 27(2)$; $K_c = 201(22)$ GPa, $K_c' = 36(9)$. These values clearly reveal the diverse character of the bonding interactions present, with the solid being virtually incompressible along c, the polymer chain direction (Fig. 4) of the bridging covalent C–C bonds ($\alpha_c = 0.0050(5)\,\mathrm{GPa}^{-1}$). On the other hand, the largest value of the compressibility is exhibited along the interchain direction, b ($\alpha_b = 0.040(5)\ \mathrm{GPa}^{-1}$) with that along a assuming an intermediate value ($\alpha_a = 0.0125(1)\ \mathrm{GPa}^{-1}$), reflecting the steric influence of the Cs^+ ions at the ($\frac{1}{2}$, 0, 0) sites.

CONCLUSIONS

In conclusion, we have presented synchrotron X-ray and neutron powder diffraction structural measurements on the ternary Na_2CsC_{60} fulleride at both ambient and elevated pressures. Na_2CsC_{60} differs markedly from other Na-containing fulleride salts as no evidence for a symmetry-lowering structural phase transition is found at ambient pressure,

with its structure remaining strictly cubic, even after prolonged standing at 200 K. Such behavior is rationalized in terms of the somewhat increased interfullerene contact distances and the inappropriate fullerene orientations in the primitive cubic phase which preclude C–C bond formation between fullerene units and subsequent polymerisation in Na_2CsC_{60}. The primitive cubic phase survives upon application of pressure to ≈ 0.76 GPa when a transition to the monclinic polymeric phase is found to occur. This is accompanied by a large decrease in volume, resulting in a strongly anisotropic tightly packed fulleride phase. The structure is essentially incompressible along the direction of the chain axis and most compressible along the interchain direction. The cubic phase completely disappears at ≈ 1.12 GPa with the polymer phase surviving to 8.63 GPa, the highest pressure of the present experiment.

ACKNOWLEDGMENTS

K.P. thanks the Leverhulme Trust for a 1997–1998 Research Fellowship. We acknowledge financial support by the TMR Programme of the European Commission (Research Network "FULPROP" ERBFMRXCT970155). We thank the ESRF for provision of synchrotron X-ray beamtime, the Rutherford Appleton Laboratory for neutron beamtime, K. Kordatos for the synthesis of the Na_2CsC_{60} sample, M. Hanfland and D. Häusermann for help with the high-pressure synchrotron X-ray measurements, and R. Smith for help with the high pressure neutron diffraction measurements.

REFERENCES

1. K. Prassides, *Current Opin. Solid State Mater. Sci.* **2,** 433 (1997).
2. O. Gunnarsson, *Rev. Mod. Phys.* **69,** 575 (1997).
3. M. J. Rosseinsky, *Chem. Mater.* **10,** 2665 (1998).
4. T. Yildirim, O. Zhou, and J. E. Fischer, *in* "Fullerene-based Materials" (W. Andreoni, Ed.). Kluwer Academic Publishers, Dordrecht, in press.
5. P. W. Stephens, L. Mihaly, P. L. Lee, R. L. Whetten, S. M. Huang, R. Kaner, F. Deiderich, and K. Holczer, *Nature* **351,** 632 (1991).
6. K. Kniaz, J. E. Fischer, Q. Zhu, M. J. Rosseinsky, O. Zhou, and D. W. Murphy, *Solid State Commun.* **88,** 47 (1993).
7. K. Prassides, C. Christides, I. M. Thomas, J. Mizuki, K. Tanigaki, I. Hirosawa, and T. W. Ebbesen, *Science* **263,** 950 (1994).
8. P. W. Stephens, G. Bortel, G. Faigel, M. Tegze, A. Janossy, S. Pekker, G. Oszlanyi, and L. Forro, *Nature* **370,** 636 (1994).
9. A. M. Rao, P. Zhou, K. A. Wang, G. T. Hager, J. M. Holden, Y. Wang, W. T. Lee, X. X. Bi, P. C. Eklund, D. S. Cornett, M. A. Duncan, and I. J. Amster, *Science* **259,** 955 (1993).
10. Y. Iwasa, T. Arima, R. M. Fleming, T. Siegrist, O. Zhou, R. C. Haddon, L. J. Rothberg, K. B. Lyons, H. L. Carter, A. F. Hebard, R. Tycko, G. Dabbagh, J. J. Krajewski, G. A. Thomas, and T. Yagi, *Science* **264,** 1570 (1994).
11. M. Nunez-Regueiro, L. Marques, J. L. Hodeau, O. Bethoux, and M. Perroux, *Phys. Rev. Lett.* **74,** 278 (1995).
12. K. Prassides, *in* "Fullerene-based Materials" (W. Andreoni, Ed.). Kluwer Academic Publishers, Dordrecht, in press.
13. K. Prassides, K. Vavekis, K. Kordatos, K. Tanigaki, G. M. Bendele, and P. W. Stephens, *J. Am. Chem. Soc.* **119,** 834 (1997).
14. G. Oszlányi, G. Baumgartner, G. Faigel, and L. Forro, *Phys. Rev. Lett.* **78,** 4438 (1997).
15. Q. Zhu, *Phys Rev. B* **52,** R723 (1995).
16. K. Tanigaki, T. W. Ebbesen, S. Saito, J. Mizuki, J. S. Tsai, Y. Kubo, and S. Kuroshima, *Nature* **352,** 222 (1991).
17. R. M. Fleming, A. P. Ramirez, M. J. Rosseinsky, D. W. Murphy, R. C. Haddon, S. M. Zahurak, and A. V. Makhija, *Nature* **352,** 787 (1991).
18. T. Yildirim, J. E. Fischer, R. Dinnebier, P. W. Stephens, and C. L. Lin, *Solid State Commun.* **93,** 269 (1995).
19. K. Tanigaki, M. Kosaka, T. Manako, Y. Kubo, I. Hirosawa, K. Uchida, and K. Prassides, *Chem. Phys. Lett.* **240,** 627 (1995).
20. K. Tanigaki and K. Prassides, *J. Mater. Chem.* **5,** 1515 (1995).
21. J. Robert, P. Petit, T. Yildirim, and J. E. Fischer, *Phys. Rev. B* **57,** 1226 (1998).
22. Y. Maniwa, T. Saito, K. Kume, K. Kikuchi, I. Ikemoto, S. Suzuki, Y. Achiba, I. Hirosawa, and K. Tanigaki, *Phys. Rev. B* **52,** R7054 (1995).
23. J. Mizuki, M. Takai, H. Takahashi, N. Môri, I. Hirosawa, K. Tanigaki, and K. Prassides, *Phys Rev. B* **50,** 3466 (1994).
24. C. M. Brown, T. Takenobu, K. Kordatos, K. Prassides, Y. Iwasa, and K. Tanigaki, *Phys. Rev. B* **59,** 4439 (1999).
25. K. Prassides, K. Tanigaki, and Y. Iwasa, *Physica C* **282,** 307 (1997).
26. G. M. Bendele, P. W. Stephens, K. Prassides, K. Vavekis, K. Kordatos, and K. Tanigaki, *Phys. Rev. Lett.* **80,** 736 (1998).
27. L. Cristofolini, K. Kordatos, G. A. Lawless, K. Prassides, K. Tanigaki, and M. P. Waugh, *Chem. Commun.* 375 (1997).
28. A. Lappas, C. M. Brown, K. Kordatos, E. Suard, K. Tanigaki, and K. Prassides, *J. Phys.: Condens. Matter* **11,** 371 (1999).
29. J. Rodriguez-Carvajal, Program Fullprof (version 3.5, Dec. 97). ILL (unpublished).
30. J. K. Cockcroft, Program Profile. Birkbeck College, London, UK, 1994.
31. W. I. F. David, D. E. Akporiaye, R. M. Ibberson, and C. C. Wilson, Rutherford Appleton Laboratory Report RAL-88-103, 1988.
32. S. Margadonna, C. M. Brown, A. Lappas, K. Kordatos, K. Tanigaki, K. Prassides, *in* "Electronic properties of novel materials. Progress in molecular nanostructures" (H. Kuzmany, J. Fink, M. Mehring, and G. Roth, Eds.), Vol. 442, p. 327. American Institute of Physics Conference Proceedings. AIP, New York, 1998.
33. S. Margadonna, C. M. Brown, K. Kordatos, A. Lappas, K. Prassides, M. Kosaka, K. Tanigaki, *in* "Recent Advances in the Chemistry and Physics of Fullerenes and Related Materials" (K. M. Kadish and R. S. Ruoff, Eds.), Vol. 6, p. 650. Electrochemical Society. Pennington, NJ, 1998.
34. B. Sundqvist, O. Andersson, A. Lundin, and A. Soldatov, *Solid State Commun.* **93,** 109 (1995).
35. C. Christides, K. Prassides, D. A. Neumann, J. R. D. Copley, J. Mizuki, K. Tanigaki, I. Hirosawa, and T. W. Ebbesen, *Europhys. Lett.* **24,** 755 (1993).
36. O. Zhou, G. B. M. Vaughan, Q. Zhu, J. E. Fischer, P. A. Heiney, N. Coustel, J. P. McCauley, and A. B. Smith, *Science* **255,** 833 (1992).
37. J. Diederichs, J. S. Schilling, K. W. Herwig, and W. B. Yelon, *J. Phys. Chem. Solids* **58,** 123 (1997).
38. F. D. Murnaghan, *Proc. Natl. Acad. Sci. U.S.A.* **30,** 244 (1947); J. R. Macdonald and D. R. Powell, *J. Res. Natl. Bur. Stand. A* **75,** 441 (1971).